Solid-liquid critical behavior of water in nanopores

Kenji Mochizuki * **and Kenichiro Koga** *

*Department of Chemistry, Faculty of Science, Okayama University, Okayama 700-8530, Japan

mochizuki@okayama-u.ac.jp and koga@okayama-u.ac.jp

Submitted to Proceedings of the National Academy of Sciences of the United States of America

Nano-confined liquid water can transform into low-dimensional ices whose crystalline structures are dissimilar to any bulk ices and whose melting point may significantly rise with reducing the pore size, as revealed by computer simulation and confirmed by experiment. One of the intriguing, and as yet unresolved, questions concerns the observation that the liquid water may transform into a low-dimensional ice either via a first-order phase change or without any discontinuity in thermodynamic and dynamic properties, which suggests the existence of solid-liquid critical points in this class of nano-confined systems. Here we explore the phase behavior of a model of water in carbon nanotubes in the temperature-pressure-diameter space by molecular-dynamics simulation and provide unambiguous evidences to support solid-liquid critical phenomena of nanoconfined water. Solid-liquid first-order phase boundaries are determined by tracing spontaneous phase separation at various temperatures. All the boundaries eventually cease to exist at the critical points and there appear loci of response function maxima, or the Widom lines, extending to the supercritical region. The finite-size scaling analysis of the density distribution supports the presence of both first-order and continuous phase changes between solid and liquid. At around the Widom line there are microscopic domains of two phases and continuous solid-liquid phase changes occur in such a way that the domains of one phase grow and those of the other evanesce as the thermodynamic state departs from the Widom line.

solid-liquid critical phenomena | water | quasi-one dimension

Abbreviations: MD, molecular dynamics

The possibility of the solid-liquid critical point has been reported by computer simulation studies of various systems in quasi-one, quasi-two, and three dimensions that exhibit both continuous and discontinuous changes in thermodynamic functions and other order parameters [1, 2, 3, 4, 5, 6, 7]. Yet the idea that a solid-liquid phase boundary never terminates at the critical point is still commonly accepted as a law of nature, largely because of the famous symmetry argument [8, 9] together with the lack of experimental observations. Furthermore, critical phenomena in quasi-one-dimensional systems are often considered impossible from a different point of view, that is, to begin with, there is no first-order phase transition in one-dimensional systems as proved for solvable models [10] or shown by the phenomenological argument [11]. Therefore a thorough investigation is much needed to support or reject the possibility of the solid-liquid critical point. We examine the phase behavior of a model system of water confined in a quasi-one-dimensional nanopore [1, 12, 13, 14, 15, 16] and provide evidences to support the existence of first-order phase transitions and solid-liquid critical points.

Significance

It is commonly believed that the solid-liquid critical point does not exist, because of the famous symmetry argument and the lack of experimental observation so far. But recently the intriguing possibility of the critical point has been suggested for strongly confined substances. Here we perform molecular dynamics simulations of a model system of water confined in carbon nanotubes and provide unambiguous evidences of the solid-liquid critical point for water confined in the quasi-one-dimensional hydrophobic nanopore: macroscopic solid-liquid phase separation below a critical temperature T_c, diverging heat capacity and isothermal compressibility at around T_c, and the loci of response function maxima above T_c. We also give a molecular-level explanation for how liquid water continuously freezes to ice in nanopores when it is cooled along a thermodynamic path avoiding the first-order phase boundary.

Reserved for Publication Footnotes

Results and Discussions

First, we explore possible solid-liquid critical points of the confined water by calculating isotherms in the "pressure-volume" plane, where the pressure is actually P_{zz} a component of pressure tensor along the tube axis, or simply the axial pressure, and the "volume" is ℓ_z the length of simulation cell in the axial direction per molecule. The isotherms are obtained by extensive canonical ensemble (NVT) molecular dynamics (MD) simulations of the TIP4P model of $N = 720$, 900 and 1080 water molecules encapsulated in model single-walled carbon nanotubes (see Methods for details). Note that direct calculations of isotherms have provided compelling evidence of the liquid-liquid phase transition in models of supercooled water [17, 18, 19]. Plotted in Fig. 1a,b,d, and e are the isotherms in the P_{zz}, ℓ_z plane at the nanotube diameter D =11.1 Å and 12.5 Å. In any cases examined, the isotherms at low temperatures have a horizontal portion in which P_{zz} does not change with ℓ_z, i.e., $dP_{zz}/d\ell_z = 0$. This indicates that the system undergoes a phase separation under these conditions [20]. (If the system size in the axial direction is small, a *van der Waals* loop will appear [18, 19].) At high temperatures the slope of the isotherms is always negative, i.e., $dP_{zz}/d\ell_z < 0$. A critical point, if exists, must be located between the highest-temperature isotherm with $dP_{zz}/d\ell_z = 0$ and the lowest-temperature isotherm without the horizontal portion. In addition, we can judge whether two phases coexist or not from the local density profile defined below. Using this approach, we locate two solid-liquid critical points for water in a nanotube of $D = 11.1$ Å at $(T_c/\mathrm{K}, P_c/\mathrm{GPa}) = (265\pm 5, 0.13\pm 0.02)$ and $(325\pm 5, 2.52\pm 0.02)$ and four critical points for $D = 12.5$ Å at $(T_c/\mathrm{K}, P_c/\mathrm{GPa}) = (287\pm 2, 0.12\pm 0.03)$, $(287\pm 2, 0.33\pm 0.04)$, $(337\pm 2, 1.49\pm 0.03)$ and $(345\pm 5, 5.16\pm 0.01)$, as indicated by red marks in Fig. 1.

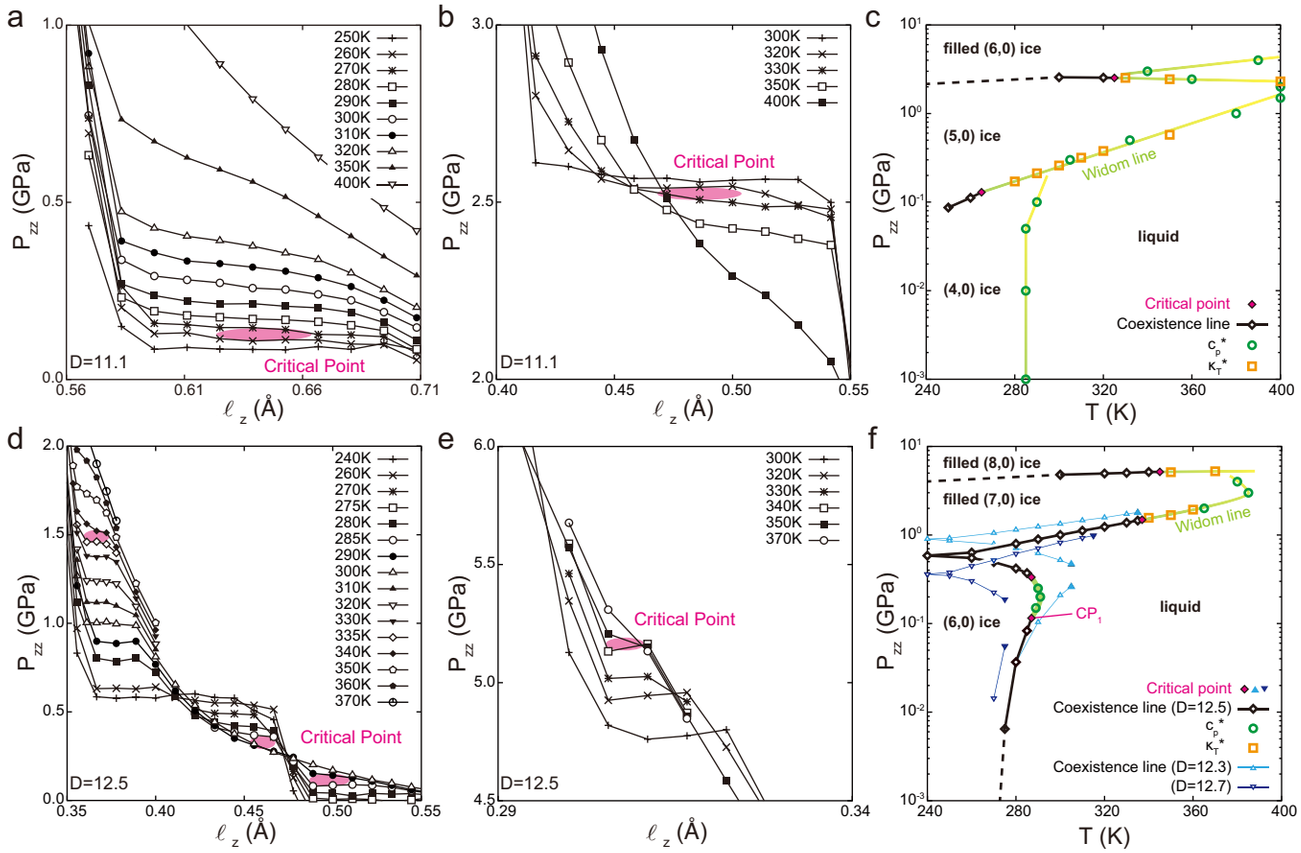

Fig. 1. Simulation results for "pressure-volume" isotherms and phase diagrams of water confined in a quasi-one-dimensional hydrophobic nanopore (a model pore of carbon nanotube). (a)(b) P_{zz}-ℓ_z isotherms and (c) T-P_{zz} phase diagram at $D = 11.1$ Å. (d)(e) P_{zz}-ℓ_z isotherms and (f) T-P_{zz} phase diagram at $D = 12.5$ Å along with those at $D = 12.3$ Å and 12.7 Å for $P_{zz} < 2.5$ GPa. The first-order phase boundaries (solid lines) in (c) and (f) are determined by the isotherms in (a)(b) and (d)(e), and those which extend to lower temperatures (dashed lines) ultimately go to the phase boundaries at $T = 0$ K determined by the pressure-dependent enthalpy H for the corresponding ices (Fig. S1) and the one extending to lower pressures [another dashed line in (f)] goes to the melting temperature at $P_{zz} = 0.1$ MPa [12]. The Widom lines drawn here are loci of maximum heat capacity c_p^* and maximum isothermal compressibility κ_T^*. The color of the Widom lines indicates the relative magnitude of c_p^*: the larger c_p^* the darker the green color.

Figure 1c and f show the T-P_{zz} phase diagram at $D = 11.1$ Å and 12.5 Å, respectively. The coexistence lines (first-order phase boundaries) in the diagram are determined from the average P_{zz} of the horizontal portion of each isotherm at a given temperature. The solid-liquid coexistence lines as obtained this way either start from the low temperature limit, where they are solid-solid phase boundaries, or branch from a solid-solid-liquid triple point; but all of them ultimately terminate at one of the solid-liquid critical points. We identify five ice phases [square, pentagonal, hexagonal, heptagonal, and octagonal ice nanotubes whose structures are specified by the roll-up vectors (4,0), (5,0), (6,0), (7,0), and (8,0), respectively [12]] and a liquid phase from the hydrogen-bond structures (Fig. 2), and we obtain the structure factor of oxygen atoms in the axial direction, the mean square displacement of molecules, and the reorientational correlation function (Fig. S2). At high pressures around 1 GPa and above, in both nanotubes of $D = 11.1$ Å and 12.5 Å, the inner space of (6,0), (7,0), and (8,0) ice nanotubes is filled with water molecules: these are indicated as "filled" ice in Fig. 1 and shown in Fig. 2. The additional water molecules intrude these ice nanotubes at high pressures because otherwise the external n-membered rings ($n = 6$, 7, 8) of water molecules would have collapsed due to strong repulsive force acting on them from the nanotube wall (Fig. S3).

Figure 1f shows how the phase boundaries shift when the nanotube diameter D is slightly reduced or enlarged from 12.5 Å (the isotherms in the P_{zz}, ℓ_z plane are shown in Fig. S4). Each ice region in the T-P_{zz} phase diagram moves upward (to higher pressure) as D decreases. Reducing D further make narrower ice nanotubes, the (5,0) and (4,0) ice

phases shown in Fig. 1c, emerge in a low pressure region under the (6,0) ice phase. The hollow space inside the (6,0) ice nanotube is empty when $D = 12.5$ Å, partially filled when $D = 12.3$ Å, and fully filled when $D = 11.1$ Å, which suggests that the empty (6,0) ice can continuously transform into filled (6,0) ice (Fig. S5). In principle the phase behavior of water confined to the cylindrical nanopores is characterized by a three-dimensional phase diagram, e.g., the T-P_{zz}-D diagram, in which the solid-liquid phase boundaries and the critical points form surfaces and their edges, respectively, and the heat capacity and the compressibility maxima, or the Widom lines [21], also form surfaces extending from the edges.

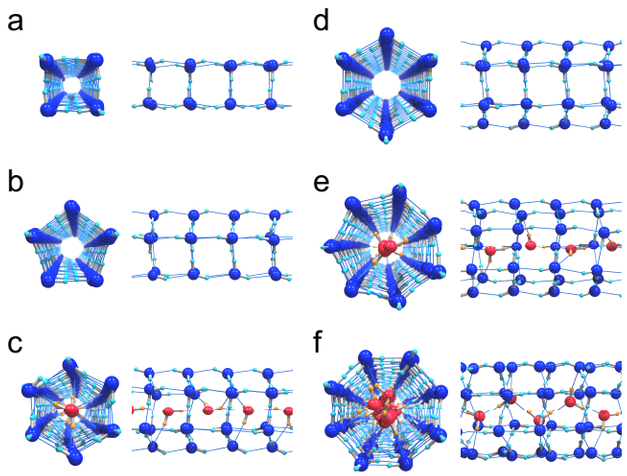

Fig. 2. Inherent hydrogen-bond structures of six ices formed in the nanotubes (a) (4,0) ice obtained from the NPT-MD trajectory at (T/K, P_{zz}/MPa)=(250, 50), (b) (5,0) ice at (230, 200) and (c) filled (6,0) ice at (270, 2700) at $D = 11.1$ Å, and (d) (6,0) ice at (280, 10), (e) filled (7,0) ice at (280, 800) and (f) filled (8,0) ice at (280, 5100) at $D = 12.5$ Å. Top views and the corresponding side views are drawn abreast. Central water molecules forming a chain in the filled ices are colored red to distinguish them from the exterior rings.

To confirm spontaneous phase separations and to observe density fluctuations near the critical points, we use the scaled local density defined as [17] $\rho(z,t) = (\Delta N(z,t)/\Delta z)\,\ell_z$, where ΔN is the number of molecules in a cylindrical slab of width Δz centered at z and ℓ_z^{-1} is the average number of molecules per unit length. Figure 3a–c show the time evolution of $\rho(z,t)$ of water in the nanotube of $D = 12.5$ Å obtained by the NVT-MD simulation at $T = 300$ K, 290 K and 280 K and at fixed volume ($\ell_z = 0.50$ Å). Note the density of the system is between those of liquid water and (6,0) ice. The initial configuration at $t = 0$ is a randomly generated one. At 300 K, a temperature above the (6,0) ice-liquid critical point (CP_1), $\rho(z,t)$ is almost uniform anywhere in the nanotube, indicating that the system is indeed homogeneous. In contrast, at 280 K, a temperature below CP_1, multiple nucleation events of (6,0) ice take place as soon as the NVT-MD run starts (Fig. 3c) [22]. Then, the embryos of (6,0) ice quickly grow and merge with each other, reflected in the initial large decrease in the water-water interaction energy U_{ww} (Fig. 3d), and spontaneous ice-water phase separation is completed around $t = 2$ ns. After that the two phases remain to coexist with their domain sizes nearly unchanged. Figure 3e shows typical structure of a water nanotube at 280 K, which clearly demonstrates the coexistence of solid and liquid phases. The spontaneous phase separation observed in the NVT-MD simulation is a direct evidence of the solid-liquid first-order phase transition.

At 290 K, a temperature close to CP_1, two kinds of domains are distinguishable (Fig. 3b); however, the domain size of (6,0) ice fluctuates with large amplitudes, which is reflected in large fluctuations in U_{ww} at 290 K (Fig. 3d). The ice-like domains have a large variety of sizes but they do not tend to merge, e.g., see three ice domains at $t = 10.5$ ns. Instead, the sudden formation and disappearance of (6,0) ice domains occur intermittently. Even a domain of (6,0) ice as large as 100 Å hardly persist over 20 ns. That is, freezing and melting seem to proceed without free energy barriers. These behaviors, clearly different from those at the higher and lower temperatures, are characteristic of critical phenomena: See Supplementary Video 1 showing the large fluctuations of the hydrogen-bond structure in a trajectory at 290 K. It is also confirmed that the system exhibits the large fluctuations of the local density at that temperature even when the trajectory starts from the solid-liquid coexisting configuration obtained at a lower temperature (Fig. S6).

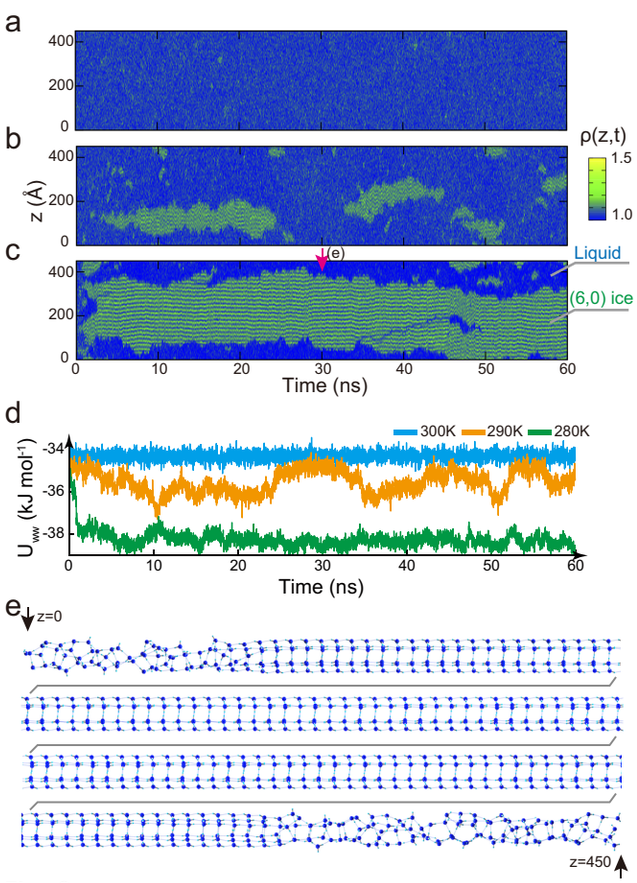

Fig. 3. Fluctuations above, near, and below the temperature of the solid-liquid critical point. (a)-(c) Time evolution of the scaled local density $\rho(z,t)$ for trajectories at 300 K, 290 K and 280 K obtained from the NVT-MD simulation ($N = 900$) with fixed density ($\ell_z = 0.5$ Å) and tube diameter ($D = 12.5$ Å). The width Δz of a bin with which the local density is defined is taken to be 5 Å. The color for $\rho(z,t) < 1$ is the same as that for $\rho(z,t) = 1$. (The raw $\rho(z,t)$ descriptions are shown in Fig. S7.) (d) Time evolution of the potential energy between water molecules (U_{ww}). (e) Inherent hydrogen-bond structure at 30 ns of the 280 K trajectory [(c)].

To verify the presence of the solid-liquid critical point, we implement the finite-size analysis of the Challa-Landau-Binder parameter $\Pi \equiv 1 - \langle\alpha^4\rangle/3\langle\alpha^2\rangle^2$ [23, 24, 25] of the density $\alpha = N/\pi\sigma^2 L_z$, where σ is the radius at which the potential energy of nanotube-water interaction is zero (Fig. S8) and L_z is the length of nanotube. The parameter Π quantifies the bimodality in the density distribution function $Q(\alpha)$. Minimum of Π along an isobar, denoted as $\Pi_{\rm min}$, approaches 2/3 as $N \to \infty$ when $Q(\alpha)$ in the thermodynamic limit is unimodal whereas $\Pi_{\rm min}$ approaches a value less than 2/3 when $Q(\alpha)$ is bimodal. We calculate Π along two isobars at D=11.1 Å: the P_{zz} = 130 MPa isobar that passes in the vicinity of an ice-water critical point inferred by the set of isotherms in Fig. 1a and the 500 MPa isobar that crosses the Widom line identified by the calculations of the heat capacity and the compressibility as shown below. For each state at 130 MPa in a range of T = 250 K and 280 K, Π is calculated from an isothermal-isobaric (NPT) MD run of 2 μs or longer for the systems of N=100, 200 and 300. Such a long MD run is required to observe phase flipping between solid and liquid phases. For each state along the 500 MPa isobar in a range of T = 320 K and 350 K, the NPT-MD run of 100 ns is sufficient for the system of N=100, 200, 300, 400 and 500. The interval of T is set to 2 K near $\Pi_{\rm min}$. Figure 4a and 4b show the change of $Q(\alpha)$ of the system with N = 300 at selected temperatures along the two isobars. At 500 MPa the density distribution $Q(\alpha)$ is unimodal and its center simply moves to a lower density with increasing temperature whereas at 130 MPa $Q(\alpha)$ becomes bimodal or widespread at temperatures between 262 K and 274 K. Figure 4c shows the finite-size scaling of $\Pi_{\rm min}$. At 500 MPa it approaches 2/3 linearly with $1/N$, indicating the absence of a first-order phase transition in the thermodynamic limit. At 130 MPa, on the other hand, $\Pi_{\rm min}$ approaches a value clearly smaller than 2/3, proving the presence of a first-order phase transition. Thus, the finite-size scaling analysis too supports the solid-liquid critical point of water confined in the quasi-one-dimensional hydrophobic nanopore.

To investigate the nature of continuous solid-liquid phase changes, we perform long-time NPT-MD simulations for the systems of N = 200 at states on isobaric paths along which continuous phase changes are observed; the production run at each state is 80 ns. First, we focus on the (configurational part of) isobaric heat capacity c_p obtained from $(\overline{H^2} - \overline{H}^2)/k_{\rm B}T^2$, the fluctuations in H defined as $U + P_{zz}\pi\sigma^2 L_z$ with U the potential energy of the system. It is confirmed that there is a maximum heat capacity ${c_p}^*$ for each isobaric path (Fig. S9). Plotted in Fig. 5a, b are $H(T)$ and $c_p(T)$ at P_{zz}= 500, 1000, 1500 MPa in the pore of D = 11.1 Å, where the continuous freezing to (5,0) ice is observed. The lower the pressure P_{zz}, the larger the heat capacity maximum c_p^* and the lower the temperature T^* of the maximum heat capacity, which is consistent with the maximum slope of $H(T)$ at T^* being steeper as reducing P_{zz}. The loci $T^*(P_{zz})$ of the heat capacity maxima ${c_p}^*$ are plotted in the T-P_{zz} phase diagram (Fig. 1c, f). Each locus of ${c_p}^*$ is smoothly connected with a locus of the solid-liquid first-order transitions. An exception is the locus between (4,0) ice and liquid phases, which extends up to a lowest pressure examined for D=11.1 Å but would be connected with the first-order boundary in a phase diagram for smaller D. In one case, two loci of ${c_p}^*$ and one first-order phase boundary seem to meet at a critical point (Fig. 1c); in the other, endpoints of two first-order boundaries are connected with a locus of the heat capacity maxima (Fig. 1f). Next, the isothermal compressibility $\kappa_T \equiv -(\partial\ell_z/\partial P_{zz})_T/\ell_z$ in the axial direction is obtained along isotherms in Fig. 1a, b, d, and e by fitting the third order polynomial function to each P_{zz}-ℓ_z curve, and the loci $P_{zz}^*(T)$ of the maximum isothermal compressibility κ_T^* are determined. The result is shown in the T-P_{zz} phase diagram (Fig. 1c,f). Each locus of the maximum compressibility is smoothly connected with a first-order phase boundary, as in the case of c_p^*. It is confirmed that the values of maxima κ_T^* and c_p^* increase as the endpoint of the first-order phase boundary is approached. There are at least three loci of κ_T^* that coincide with loci of c_p^*. Recently, Luo et al. [26] have shown that near the critical point, in general, the loci of maximum c_p and κ_T converge into a single line, the Widom line [21]. Thus, the behaviors of the response function maxima presented here suggest the existence of the solid-liquid critical points and the Widom lines. Note that each ice phase [except (8,0) ice] is enclosed by the coexistence lines and the Widom lines, or the loci of c_p^* and κ_T^*.

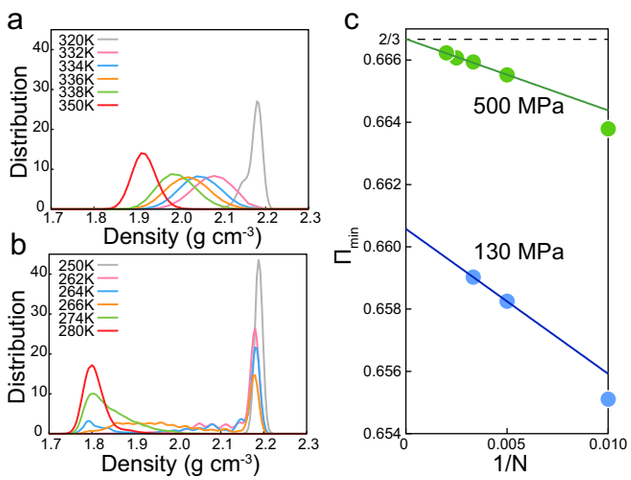

Fig. 4. Finite-size scaling analysis of the Challa-Landau-Binder parameter of the density distribution function $Q(\alpha)$. (a)(b) $Q(\alpha)$ at selected temperatures for 500 MPa and 130 MPa, respectively. The temperature at which the $Q(\alpha)$ gives a minimum Π ($\Pi_{\rm min}$) is 336 K at 500 MPa and 264 K at 130 MPa. (c) Finite-size scaling of $\Pi_{\rm min}$ along isobars of 130 MPa and 500 MPa: $\Pi_{\rm min}$ vs. $1/N$. At 500 MPa, $\Pi_{\rm min}$ approaches 2/3+0.0001 (a linear fit to the data of N=200, 300, 400 and 500). At 130 MPa, $\Pi_{\rm min}$ approaches 0.660 (a linear fit to the data of N=200 and 300).

Now we examine how dynamic and structural properties of water change as it continuously freezes in (5, 0) ice, by crossing the Widom lines or the loci of c_p^* and κ_T^*. Figure 5c shows temperature dependence of the diffusion coefficient of water along the tube axis ($D_z = \lim_{t\to\infty} \overline{|z(t) - z(0)|^2}/2t$). There are three stages through which the dynamic property D_z changes: the most rapid change in D_z is observed in the intermediate range which include the temperature T^* of maximum heat capacity. For limited ranges at higher or lower T, one may find an Arrhenius behavior in D_z, but overall D_z is non-Arrhenius. The static structure factor $S(q)$ of oxygen atoms along the z-axis also shows a three-stage variation with T. The first peak of $S(q)$ appears at around $q = 0.35$ Å^{-1} corresponding to the lattice spacing of ice nanotubes in the axial direction. The peak intensity $\hat{S}(T)$ given by integrating the local spectrum $S(q)$ around the first peak is plotted in Fig. 5d, which indicates that with increasing T the ordered crystalline structure disappear continuously, and it happens most rapidly in the intermediate range of T. That intermediate range coincides with the range in which D_z varies most rapidly and c_p

has a maximum. The temperature range of the intermediate stage shrinks as the critical point is approached.

How can the crystalline ices gradually transform to liquid water? Further analysis of the hydrogen-bond structures reveals that there is a sort of microscopic phase separation in the intermediate stage, where microscopic ice-like and liquid-like domains coexist (Fig. 5e). That is, the continuous melting observed for the nanoconfined water does not mean that there are homogeneous intermediate structures between an ice crystal and liquid water; rather, the ice-like and liquid-like domains in microscopically inhomogeneous states grow and disappear continuously. The existence of interfaces between ice and liquid water in the intermediate stage means that the associated interfacial tension is too small to promote macroscopic phase separation. This in turn indicates that microscopic structures of liquid water confined in nanopores can be similar to those of ice under certain conditions [1, 3]. The three-stage transformation found here is different from the dynamic crossover observed in supercooled water (a sharp change from an Arrhenius to a non-Arrhenius behavior of the diffusion constant at T^*) [21]. The behavior found here is rather similar to that observed in a supercritical Lennard-Jones fluid [27], although there are some qualitative differences.

There is a famous argument for the non-existence of the solid-liquid critical point based on the assertion that a particular symmetry exists or does not exist [9]. The argument is, however, not unassailable, since, for example, one may conceive that defects in a solid increase in number continuously upon heating until the whole system is rendered disordered. And this is exactly what we observe for the quasi-one-dimensional ices. Figure S10 shows the fraction of defects in pentagonal ice nanotube as a function of T and the density distributions of water molecules in the cross section of the pore at four temperatures. The fraction of defects in ice is 1.5 % at 150 K, and decreases to 0.7 % at 100 K. As the temperature goes up from 150 K to 360 K, the fraction of defects increases continuously and exceeds 60 %, and the five-fold symmetry of pentagonal ice nanotube disappears gradually. In contrast, when a bulk solid is heated, a small number of defects immediately lead to a collapse of the entire crystalline structure at a specific temperature [28, 29, 30]. Given the fact that simulated water and simple liquids may be continuously transformed to ordered solids in quasi-one-dimensional [1, 4] and quasi-two-dimensional nanopores [3, 6] while such gradual transformation is not observed for the bulk systems, we suspect that a decisive factor enabling water and other simple molecules to exhibit continuous freezing is confinement.

Although the ice nanotubes at sufficiently low temperatures have perfect crystalline structures as observed in our molecular simulation, there is a possibility that the quasi-one-dimensional ices are intrinsically polycrystalline solids whose grain size is larger than a typical cell size of molecular simulation, say, 10 nm in length. Then there would be no contradiction between the solid-liquid critical phenomena and the symmetry argument.

Another commonly accepted view which seems to contradict the phase behavior reported here is that there cannot be phase transitions in one-dimensional systems with short-range interactions. It is based on either conclusions derived from exactly solvable models [10], Landau's phenomenological argument [11], or van Hove's theorem [31]. But it is established with counterexamples [32, 33, 34, 35, 36, 37] that van Hove's theorem is valid for a limited class of one-dimensional systems [31, 38], and the model system we studied here is not included in the class. Rather, ours belongs to "almost one-dimensional" systems, which may well have phase transitions [39]: it has an external field due to the cylindrical wall, intermolecular interactions in a transverse dimension in addition to those along the tube axis, and an infinite number of states for each molecule at given position z.

Among the one-dimensional models the Chui-Weeks model of interfaces [35] and the Dauxois-Peyrard-Bishop model of DNA denaturation [36, 37] seem to be most relevant to the confined water studied here: both have an infinite number of states for each 'site' in a row, assume Hamiltonian with potentials for each site and for the nearest-neighbor site-site interaction, and exhibit first-order phase transitions. Here we consider the model of DNA, as it is physically more similar to water confined in nanopore, and try to find a correspondence between the solvable model and the realistic model of confined water, which may help us better understand the observed solid-liquid phase transition. The model of DNA is a row of stacked base pairs: the i-th base pair with a stretching y_i of the hydrogen bond has a potential $V(y_i)$ and two neighboring base pairs are coupled by a potential $W(y_i, y_{i-1})$ whose anharmonicity may be tuned. With the short-range interaction W between base pairs the model of DNA exhibits the first-order melting transition. Water confined in a nanopore takes a form of stacked clusters of molecules. The potential energy of the system may be expressed as the sum of the energy $V'(Y_i)$ of the i-th cluster and the sum of the neighboring cluster-cluster interaction energy $W'(Y_i, Y_{i-1})$ with Y_i the configuration of the i-th cluster. In the lowest-energy state (n-gonal ice nanotube) each cluster forms the n-membered ring of H_2O and the rings are stacked to form the n-gonal tube while in a high-energy state clusters with dangling OH bonds are randomly stacked. Because of the apparent correspondences between V and V' and between W and W', the phase transition of confined water may well be of first-order. Furthermore, the model of DNA exhibits both continuous and first-order transitions depending on the anharmonicity in the potential W [37]. In the model water the form of the potential function W' should change with the nanotube diameter and the axial pressure. Then, the variation of W' caused by the tube diameter or pressure might be responsible for the confined water undergoing the first-order or continuous solid-liquid phase change. As remarked above there are other confined systems that exhibit both continuous and discontinuous solid-liquid phase transitions [3, 4, 6]. Phase behaviors of these quasi-one- and quasi-two-dimensional systems, too, may be understood by examining a correspondence with the solvable models [35, 36] or the two dimensional versions of such models.

To better understand the nature of the phase behavior of a class of confined fluids that exhibit both continuous and first-order solid-liquid phase changes and the associated critical phenomena, there would be several directions to pursue. In particular we propose two issues to be resolved in connection with the arguments about the solid-liquid critical point and the non-existence of phase transitions in one dimension. First, it is important to examine whether the solid phases, e.g., ice nanotubes in the present study, are truly crystalline solids or intrinsically polycrystals whose grains are not macroscopic. For this purpose, larger-scale molecular simulations and perhaps the free energy calculations of a single crystal and polycrystals may be required. Second, it is worth examining in detail a correspondence between the solvable models such as the model of DNA denaturation and the realistic model studied here. For example, it is interesting to obtain a phase diagram for the model of DNA by changing the anharmonicity in the potential W and examine the nature of the crossover between the first-order and continuous phase changes. Also it may be worthwhile to attempt to evaluate the effective potential W' in the realistic model and see whether the change in W' with the

nanotube diameter and the pressure qualitatively corresponds to the change in W in the model of DNA.

Potential applications of the robust solid-liquid critical phenomena in confined water would be to facilitate chemical reactions, control structural changes of biological molecules, and promote protein crystallization, using critical fluctuations [40] at desired temperature by choosing a suitable confining geometry and pressure.

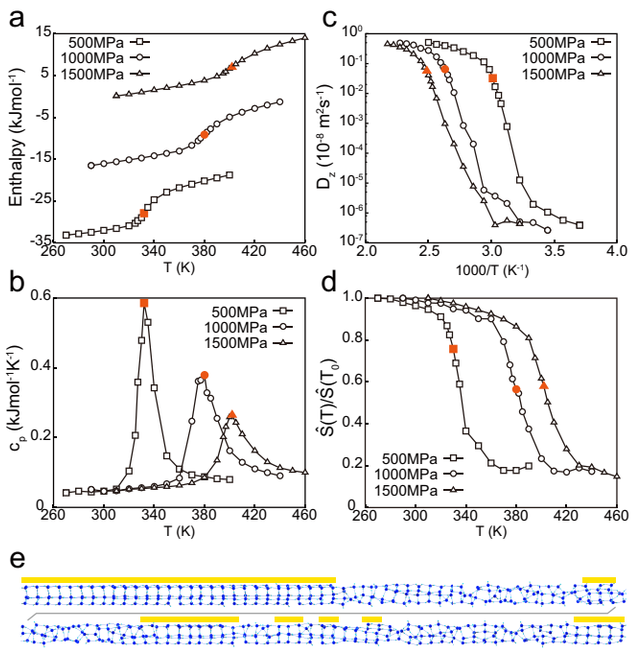

Fig. 5. The temperature (T) dependence of static and dynamical properties along the paths of continuous freezing of water into (5,0) ice in the nanotube of $D = 11.1$ Å at $P_{zz} = 500$, 1000 and 1500 MPa. Shown here are those obtained from NPT-MD simulations of 200 water molecules. (a) The configurational part of enthalpy. (b) The isobaric specific heat capacity (c_p). The temperature of maximum heat capacity T^* is 332 K for 500 MPa, 380 K for 1000 MPa and 402 K for 1500 MPa (as indicated by orange marks in **a**–**d**). (c) Arrhenius plot of the diffusion coefficient in the z direction (D_z). (d) The normalized peak intensity $\hat{S}(T)/\hat{S}(T_0)$ of the static structure factor of oxygen atoms in the z direction. The reference temperature T_0 is 270 K for 500 MPa, 290 K for 1000 MPa and 310 K for 1500 MPa. (e) The typical inherent hydrogen-bond structure obtained at T^* (332 K at 500 MPa). The islands of the ordered and the disordered structures are clearly seen. The stacked pentagonal rings, indicated by yellow, represent microscopic domains of the (5,0) ice.

Methods

We perform extensive molecular dynamics simulations in the canonical ensemble (NVT-MD) and in the isothermal-isobaric ensemble (NPT-MD) for a model system of water confined in a smooth cylindrical nanopore (a model of the single-walled carbon nanotube). A periodic boundary condition is applied in the axial direction (z-axis). The temperature T and the internal axial-pressure P_{zz} (the pressure tensor parallel to the z-axis) are controlled using modified Nośe-Andersen's method [41]. The intermolecular interaction of water is taken to be the TIP4P model [42]: the melting temperatures of the model water in carbon nanotubes are in good agreement with experimental results [12, 43, 44]. The interaction between a water molecule and the cylindrical wall is described by the Lennard-Jones potential integrated with respect to the positions of carbon atoms over the cylindrical surface with an assumption of uniform distribution of carbon atoms [1]. The nanotube diameter D is fixed to 11.1, 12.3, 12.5 and 12.7 Å: the cross-sectional potential energy profiles are shown in Fig. S8. The diameters 11.1 Å and 12.5 Å are those of the zig-zag (14,0) and (16,0) single-walled carbon nanotubes, respectively.

In the NVT-MD simulations, the number N of water molecules is 900 for the nanotubes of length $L_z = 310$–520 Å and diameter $D = 12.5$ Å, $N = 1080$ for $L_z = 312$–360 Å and $D = 12.5$ Å, $N = 900$ for all L_z and $D = 12.3$ Å and 12.7 Å, and $N = 720$ for all L_z and $D = 11.1$ Å. The highest-density examined in the simulations is $\ell_z \equiv L_z/N = 0.29$, which corresponds to P_{zz} up to 7 GPa. Confined water under such an ultra-high pressure is hardly realized in experiment; Nevertheless, the exploration into high-pressure states gives coherent understanding of the phase behavior in confined spaces. The finite-size scaling analysis is implemented by the NPT-MD simulations of the systems with N=100, 200, 300, 400 and 500. Other NPT-MD simulations are performed with $N = 200$ for most of the thermodynamic states and $N = 500$ for the states in which we observe the microscopic phase separation as shown in Fig. 5e.

Trajectories are generated by the Gear predictor-corrector method with a time step of 0.5 fs. The equilibration time of each state point in the NVT-MD simulation is at least 20 ns and 200 ns or longer at some co-existence conditions. Then, equilibrium properties are obtained from production runs of 30-90 ns. In the NPT-MD simulation, each simulation time is 100 ns for most cases and extended to a few μs for the finite-size scaling analysis. The equilibration run of 20 ns or longer is followed by the production run for analyses. The instantaneous configurations are used for the analyses except for the snapshots. For the latter, we use the inherent structures, i.e., structures obtained by applying the constant-volume steepest-descent method to the instantaneous structures visited by the trajectories.

ACKNOWLEDGMENTS. This work was supported by a Grant-in-Aid for Scientific Research (KAKENHI) (No. 26888011 and 26287099), Research Center of New Functional Materials for Energy Production, Storage and Transport at Okayama University, and the program for promoting the enhancement of research universities, MEXT. Most of the calculations were performed at the Research Center for Computational Science in Okazaki, Japan. We thanks H. Akiyoshi, K. Himoto, T. Yagasaki, T. Sumi, M. Matsumoto and H. Tanaka for their support. We are grateful to B. Widom for helpful comments.

1. Koga K, Gao G, Tanaka H, Zeng X C (2001) Formation of ordered ice nanotubes inside carbon nanotubes. Nature 412:802–805.
2. Ball P (1993) New horizons in inner space. Nature 361:297.
3. Han S, Choi M, Kumar P, Stanley H (2010) Phase transitions in confined water nanofilms. Nat. Phys. 6:685–689.
4. Koga K, Tanaka H (2006) Close-packed structures and phase diagram of soft spheres in cylindrical pores. J. Chem. Phys. 124:131103.
5. Gordillo M C, Martínez-Haya B (2006) Freezing of hard spheres confined in narrow cylindrical pores. J. Chem. Phys. 125:144702.
6. Radhakrishnan R, Gubbins K, Sliwinska-Bartkowiak M (2002) Existence of a hexatic phase in porous media. Phys. Rev. Lett. 89:076101.
7. Elenius M, Dzugutov M (2009) Evidence for a liquid-solid critical point in a simple monatomic system. J. Chem. Phys. 131:104502.
8. Stanley H (1971) Introduction to Phase Transitions and Critical Phenomena. (Oxford University Press).
9. Landau L D, Lifshits E M (1980) Statistical Physics: Course of theoretical physics. (Butterworth-Heinemann).
10. Thompson C J (1988) Classical equilibrium statistical mechanics. Oxford science publications (Clarendon Press), pp 50 and 138.
11. Landau L D, Lifshits E M (1980) Statistical Physics: Course of theoretical physics. (Betterworth-Heinemann), pp 537.

12. Takaiwa D, Hatano I, Koga K, Tanaka H (2008) Phase diagram of water in carbon nanotubes. Proc. Natl. Acad. Sci. USA 105:39–43.
13. Bai J, Wang J, Zeng X C (2006) Multiwalled ice helixes and ice nanotubes Proc. Natl. Acad. Sci. USA 103:19664–19667.
14. Byl O, et al. (2006) Unusual hydrogen bonding in water-filled carbon nanotubes J. Am. Chem. Soc. 128:12090–12097.
15. Kolesnikov A, et al. (2004) Anomalously soft dynamics of water in a nanotube: A revelation of nanoscale confinement. Phys. Rev. Lett. 93:035503.
16. Takaiwa D, Koga K, Tanaka H (2007) Structures of filled ice nanotubes inside carbon nanotubes. Mol. Simul. 33:127–132.
17. Yagasaki T, Matsumoto M, Tanaka H (2014) Spontaneous liquid-liquid phase separation of water. Phys. Rev. E 89:020301.
18. Poole P, Sciortino F, Essmann U, Stanley H (1992) Phase-behavior of metastable water. Nature 360:324–328.
19. Yamada M, Mossa S, Stanley H, Sciortino F (2002) Interplay between time- temperature transformation and the liquid-liquid phase transition in water. Phys. Rev. Lett. 88:195701.
20. Palmer J C, et al. (2014) Metastable liquid-liquid transition in a molecular model of water. Nature 510:385–388.
21. Xu L, et al. (2005) Relation between the Widom line and the dynamic crossover in systems with a liquid-liquid phase transition. Proc. Natl. Acad. Sci. USA 102:16558–16562.
22. Bhimalapuram P, Chakrabarty S, Bagchi B (2007) Elucidating the mechanism of nucleation near the gas-liquid spinodal. Phys. Rev. Lett. 98:206104.
23. Chella M S, Landau D P, Binder K (1986) Finite-size effects at temperature driven first-order transitions Phys. Rev. B 34:1841–1852.
24. Kesselring T A, Franzese G, Buldyrev S V, Hermann H, Stanley H E (2012) Nanoscale dynamics of phase flipping in water near its hypothesized liquid-liquid critical point Sci. Rep. 2:474
25. Bianco V, Franzese G Critical behavior of a water monolayer under hydrophobic confinement Sci. Rep. 4:4440
26. Luo J, Xu L, Lascaris E, Stanley H E, Buldyrev S V (2014) Behavior of the Widom line in critical phenomena. Phys. Rev. Lett. 112:135701.
27. Han S (2011) Anomalous change in the dynamics of a supercritical fluid. Phys. Rev. E 84:051204.
28. Mochizuki K, Matsumoto M, Ohmine I (2013) Defect pair separation as the controlling step in homogeneous ice melting. Nature 498:350-354
29. Forsblom M, Grimvall G (2005) How superheated crystals melt. Nat. Mater. 4:388-390
30. Jin Z H, Gumbsch P, Lu K, Ma E (2001) Melting mechanisms at the limit of superheating. Phys. Rev. Lett. 87:055703
31. Cuesta J A, Sánchez, A (2004) General non-existence theorem for phase transitions in one-dimensional systems with short range interactions, and physical examples of such transitions. J. Stat. Phys. 115:869–893.
32. Kittel C (1969) Phase transition of a molecular zipper Am. J. Phys. 36:917–920.
33. Nagle J F (1968) The one-dimensional KDP model in statistical mechanics. Am. J. Phys. 36:1114–1117.
34. Koga K (2003) Freezing in one-dimensional liquids. J. Chem. Phys. 118:7973–7980.
35. Chui S T and Weeks J D (1981) Pinning and roughening of one-dimensional models of interfaces and steps. Phys. Rev. B 23:2438–2441.
36. Dauxois T, Peyrard M, and Bishop A R (1993) Entropy-driven DNA denaturation. Phys. Rev. E 47:R44–R47.
37. Theodorakopoulos N, Dauxois T, and Peyrard M (2000) Order of the phase transition in models of DNA thermal denaturation. Phys. Rev. Lett. 85:6–9.
38. Evans M R (2000) Phase transitions in one-dimensional nonequilibrium systems. Braz. J. Phys. 30:42–57.
39. Fisher M E (1983) Walks, walls, wetting, and melting. J. Stat. Phys. 34:667–729.
40. tenWolde P R and Frenkel D (1997) Enhancement of protein crystal nucleation by critical density fluctuations. Science 277:1975–1978.
41. Rapaport D C (1997) The Art of Molecular Dynamics Simulations. (Cambridge Univ. Press, Cambridge).
42. Jorgensen W, Chandrasekhar J, Madura J, Impey R, Klein M (1983) Comparison of simple potential functions for simulating liquid water. J. Chem. Phys. 79:926–935.
43. Maniwa Y, et al. (2005) Ordered water inside carbon nanotubes: formation of pentagonal to octagonal ice-nanotubes. Chem. Phys. Lett. 401:534–538.
44. Kyakuno H, et al. (2011) Confined water inside single-walled carbon nanotubes: Global phase diagram and effect of finite length. J. Chem. Phys. 134:244501.